A COMPARATIVE STUDY ON THE PRODUCTION OF SATELLITE ORTHOIMAGERY FOR GEOLOGICAL REMOTE SENSING

Athanassios Ganas and Evangelos Athanassiou
Department of GeoInformation and Environmental Studies
Integrated Information Systems SA
72-74 Salaminos Str., 176 75 Kallithea, Athens, Greece

ABSTRACT

In most geological applications of Earth Obervation (EO) data over mountainous regions little attention is given to orthorectification, mainly because of the large spatial errors that can be tolerated (often many times the original pixel size). In most times a least-squares polynomial fit serves the purpose of image georeferencing. In this paper two procedures for optical EO data orthorectification are presented which differ on the extraction of the Digital Elevation Model (DEM). The procedures run on a commercial software package (EASI PACE v6.2.2 for Windows NT). The high-resolution DEM can be either supplied by automated stereomatching of SPOT PAN 1A imagery or by in-house digitising of 1:50,000 contour maps. A SPOT DEM has been produced for a mountainous region in central Evia (Greece) and its comparison with the reference DEM yielded satisfactory results. That ensures the fast production of accurate orthoimages for geological mapping.

INTRODUCTION

Many geologists use remotely-sensed image maps to locate themselves in the field or to draw lithological boundaries at a variety of scales. These maps are often inaccurate (in terms of accuracy as defined in topographic science; see Petrie, 1998). In most cases, planimetric errors of the order of 100-m (3 times the size of a Landsat TM pixel) can be easily tolerated because both structural measurements usually concern features of several kilometres in length (e.g., Tibaldi and Ferrari, 1988; Johnson and Harrison, 1989) and the weathered surfaces of the various rock types make the parent rock boundaries difficult to delineate without extensive field work. In fact, spatial errors of the order of 100-200 m are often tolerated because structural work with EO data is mainly concerned with the identification of long term, horizontal displacements across tonal discontinuities (lineaments) in image space, i.e. locate the strike-slip faults; and the collection of rose diagrams out of a wide range of fault populations to constrain the orientation of the principal stress axes. In addition, modelling of dynamic earth processes also makes use of coarse DEMs (100 to 500 metres; Ganas et al., 1997; Densmore et al., 1998), that effectively yields base products at 1:100,000 to 1:500,000 scales.

However, larger scale image orthorectification becomes increasingly important in EO data processing because of several new applications of geological remote sensing that require accurate image data. These new applications include : terrain visualisation (with thematic information overlain accurately in areas outside the Ground Control Points or GCPs; Dymond et al., 1992), geomorphometry (the quantitative description of landscapes), earthquake geodesy (mapping of earth surface movements associated with large earthquakes; Massonnet et al., 1993) and exploration (production of accurate land cover maps to locate seismic routes).

Orthorectification is also necessary to:
a) remove radiometric distortions induced by high relief in multitemporal, change detection studies (to correct for the so-called topographic effect), b) to reduce ground positional errors in the geometrically corrected data which are about 300 - 800 metres (TM system corrected-level 5 for Europe or SPOT 1B; Husak et al., 1999) and (c) to rectify and resample spaceborne imagery that has been acquired with off-nadir geometry such as the SPOT satellite series and side-looking SARs. Orthoimages also comprise better components for fused products and mosaics of large areas of the Earth's surface (Cheng and Toutin, 1995; Toutin, 1998).

METHODOLOGY FOR PRODUCTION OF ORTHOIMAGES

Ancillary data needed for the production of OrthoImagery are : a) Ephemeris data to establish platform orbital height and motion at the time of the overpass. These data are usually included in the header files accompanying the image data, b) a geocoded Digital Elevation Model (DEM) to rectify the image with a grid size ideally matching the EO data pixel size (i.e. 10-20 m for IRS-1C and SPOT, 30 m for TM) and c) good ground control for exterior orientation provided by differential GPS control points or from points digitised from large-scale topographic maps (usually 1:50,000).

The most difficult dataset to collect is usually the DEM. DEMs can be supplied by a) automated stereomatching of across-track stereo SPOT PAN 1A format imagery (e.g., Muller, 1989; Devereux et al., 1997; Ganas et al., 1997; see Figure 3 below) or IRS-1C stereopairs (e.g. Rao et al., 1996) and b) digitisation of large and medium-scale topographic maps produced by analog photogrammetry (Figure 1) to the appropriate raster grid. Stereomatching of Level 1A data yields superior results to those of 1B (Zoej and

Petrie, 1998). Obviously, in areas of mountainous terrain such as central Greece (38.6N-24E; see Figures 1 and 7) , the latter process (b) is more accurate only when contour sampling is total and not selective. For example, to properly orthorectify SPOT PAN data the map scale needed is 1:50,000 with a contour interval of 20 m. For a mountainous area of 40 x 40 km this requires a digitising effort of a few man-months. However, in this paper we show that spaceborne DEMs can be equally applied to orthorectify imagery at such regions, thus, reducing processing time and labour effort.

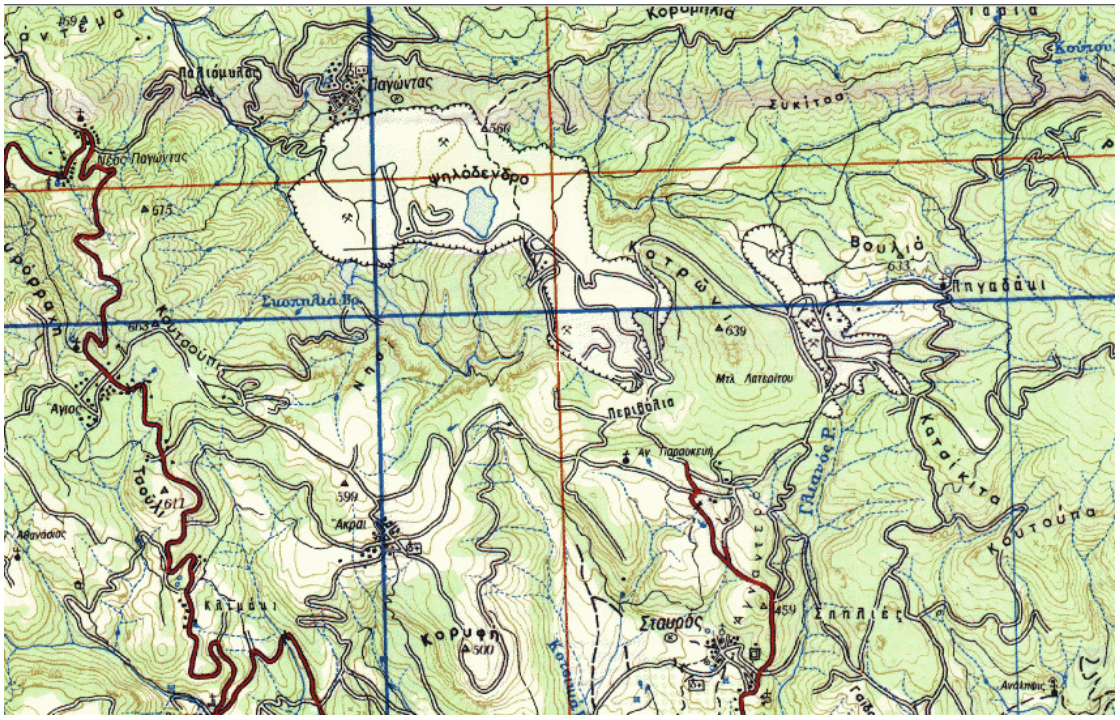

Figure 1. A subset of the georeferenced 1: 50,000 image map of central Evia (Greece) used to collect the ground control points. The source map has been produced by HAGS (1990) and its nominal accuracy is 25-m XY and 10-m Z. Areas in white is the surface extent of the ferro-nickel mines in 1990.

DEM extraction

Procedure 1) Our reference DEM is produced in house by on-screen digitising the 1:50,000 scale maps (Figure 2; contour interval 20 m) supplied by the Hellenic Army Geographical Service (HAGS). The nominal error on these maps is 5m vertical and 15 m planimetric. This error margin is tolerated for most geological applications.

The topographic map digitisation chain is :

- Scanning of the general-use map in 600 dpi to a 8-bit TIFF format (Figure 1; this step is necessary to collect the GCPs for orthorectification)
- Import of the TIFF file into the EASI PACE v6.2.2 software
- Building of Pyramid layers using a Cubic Convolution Algorithm and georeferencing using the GCPWorks module. The resultant pixel size is between 1-3 metres.
- Scanning of the contour layer in 1200 dpi to a 8-bit TIFF format

- Georeferencing of the contour layer to the Greek National Projection System (EGSA87) by use of ground control points (1st order transformation) selected at lat/lon grid intersections.
- On-screen digitising of 20-m elevation contours and production of a line vector layer (Figure 2)
- Resampling of the contour map to the desired pixel size (10 or 20 m)
- Application of the program GRDVEC to encode the lines
- Application of the Interpolation Algorithm GRDINT (Carrara, 1988) to produce the raster grid
- 3×3 filtering of the DEM for smoothing
- Manual DEM editing in areas of heavy interpolation artifacts

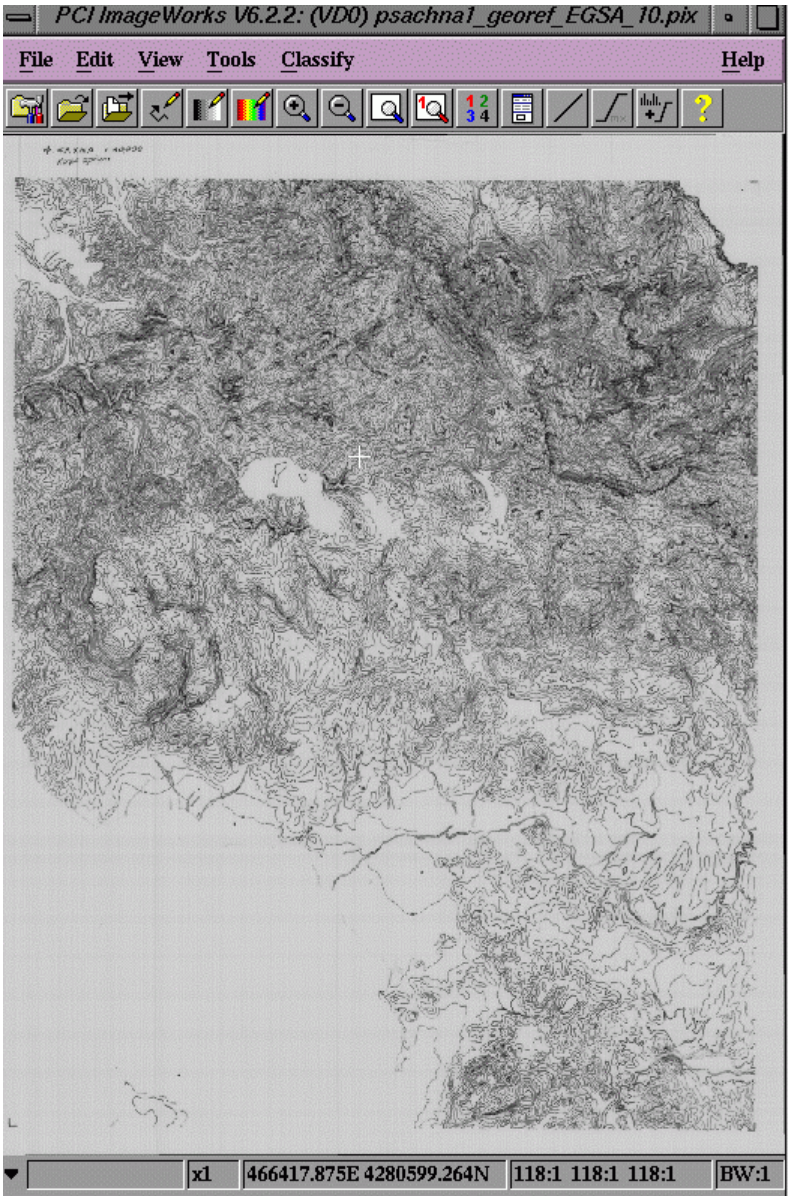

Figure 2. The vector layer of the 1:50,000 contours of central Evia (Greece) as digitised on-screen to produce the 10-m reference DEM. Contours are at 20-m intervals. Void areas in the vicinity of the white cross (centre of the layer) indicate no data (mining districts). Notice x,y,z values in the bottom.

Procedure 2) Our spaceborne DEMs are extracted from automated stereomatching of Level 1A SPOT Panchromatic images (10 m pixel size) of the area of interest, after taking into consideration the following requirements (Gugan and Dowman, 1988), in order of decreasing priority:

- availability of a high Baseline to Height ratio (B/H ≥ 0.6) stereopair,
- acquisition of either one or both scenes during high-sun angle conditions,
- acquisition interval between the stereopair scenes ≤ 30 days to assure radiometric stability and
- clear atmospheric conditions during image acquisitions.

In this paper, we show that the spaceborne method can supply accurate DEMs for the needs of producing orthoimagery. A 10-m SPOT DEM produced by IIS using the EASI/PACE v6.2.2 software has been used to rectify SPOT imagery in the Evia region, central Greece and to produce elevation maps for an active, Ferro-Nickel, mining district. The extracted DEM showed no physiographic errors (valleys and ridges appear with identical patterns to the reference DEM) and it attained z-RMS errors of about 15 metres outside the mining district where reference data exist. This error is attributed to the lack of proper GCPs (road intersections) inside the part of this area with rugged relief (0-1300 m).

SPOT PAN stereomatching

The systematic sampling of elevations can be extracted from satellite stereopairs if two things are known : image geometry (model) and the X and Y displacement between matching pixels in the two images. Data on image geometry can be retrieved from ephemeris and orbital information included with the raw imagery in combination with the Earth's shape and size. A set of Ground Control Points (GCPs) usually collected from topographic maps of the area of interest is also used to orientate the satellite with respect to the ground. In EASI PACE X and Y displacements are measured by area correlation techniques where patches of pixels on either image are shifted in image space until they match perfectly. However, correlation may be affected by pushbroom noise and by surface changes between the two acquisitions, such as clouds, shadows, land cover change etc. The major technical characteristics of the image dataset used to extract the Greek DEM (Figure 3) are given in Table I.

The software used to process the SPOT PAN stereopair is the EASI PACE v6.2.2 for Windows NT. This software was found to produce systematically better results than other commercially available packages on the flat test area of the Jordanian Desert (Al-Rousan and Petrie, 1998). At present, the software runs on a 266 Pentium II computer with a 128 Mb RAM and the processing speed was rather satisfactory (the main DEM extraction module runs for 4 hours only).

The procedure of extracting a DEM from a pair of stereo SPOT images comprises the following steps:

1) CDSPOT - CD-ROM reading: this module reads SPOT imagery from a SPOTIMAGE LGSOWG format CD. CDSPOT automatically creates a PCIDSK file (specific file format of EASI PACE), reads all of the requested imagery channels from CD, and saves the satellite path information in one or two segments.

2) GCPs collection: 19 GCPs where manually collected on both images using the program GCPWorks with respect to a geocoded (reference) database (see procedure 1 above) with RMS errors of less than 0.8 of a pixel. The addition of more GCPs did not decrease

the RMS error. The reference image was a scanned, georeferenced 1:50000 map (Figure 1; Psachna Sheet, 1990). The map pixel size was 3.2 m and projection was the Greek National Geodetic System (EGSA 1987). The GCPs where distributed as evenly as possible over the images at various elevations (see Tables II and III below). No GCPs were collected within snow-covered areas, which occur mainly towards the East (Dirfis mountain range), however, this was not found to influence the results significantly (see accuracy assessment below). The EASI program GCPELEV was used to extract the elevations of the GCPs from a preconstructed, 10-m grid DEM (the reference DEM for this study area), although an option exists to insert elevations manually.

3) SMODEL - Satellite Model Calculation: Calculates the mathematical model required for orthorectification of a satellite image or for DEM extraction from two stereo SPOT images (see Al-Rousan et al., 1997 for a description of the model). The model is generated from the satellite orbit (and attitude : pitch, roll, yaw) data and Ground Control Points (GCPs). This step for both images resulted in X-Y RMS errors of about 1 pixel, very close to the GCP errors (see Tables II and III below).

4) SEPIPRO - Satellite Epipolar Projection: Creates an epipolar projection of a satellite image given a pair of stereo SPOT images. The epipolar projected image is used to measure parallax when extracting a digital elevation model from stereo images using the SDEM program. The 16011993 (Table I) scene was selected for epipolar projection.

5) SDEM - Satellite Automatic DEM Extract: Automatically extracts a digital elevation model (DEM) from a pair of stereo SPOT satellite images of the same scene and outputs the DEM to a 16-bit file. An extraction interval of 1 (every pixel) resulted in a 10-m grid DEM. In addition, the values of 0 and 1350 were assigned to the minimum and maximum elevations in the area covered by the imagery. We chose as failed DEM value and as Background Elevation Value the integers –100 and –150, respectively. Failed values appeared mainly in the sea.

6) The program SDEMCPY is used to transfer the extracted DEM to a geo-coded EGSA (Greek national projection) file. This file was reprojected to the UTM projection.

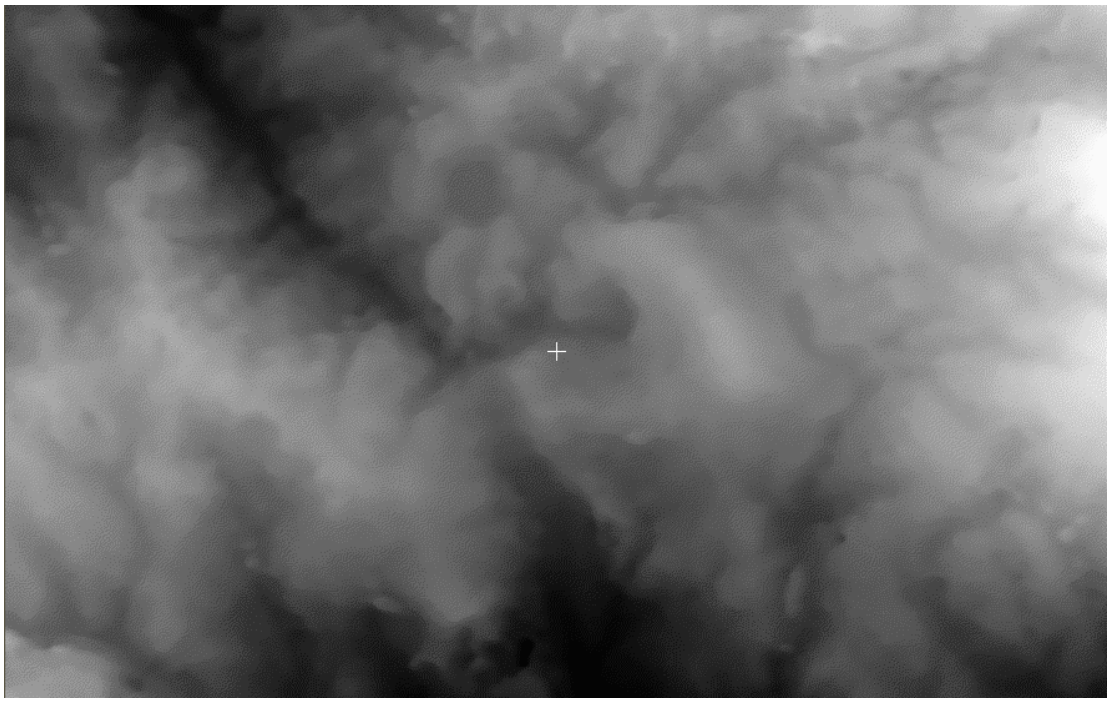

Figure 3. Intensity image showing the extracted DEM of the January-February 1993 SPOT PAN stereopair using the EASI PACE v6.2 software. Increasing brightness indicates areas of higher elevations. B/H is 1.05, data type is 16-bit Integer (signed). North is towards the top.

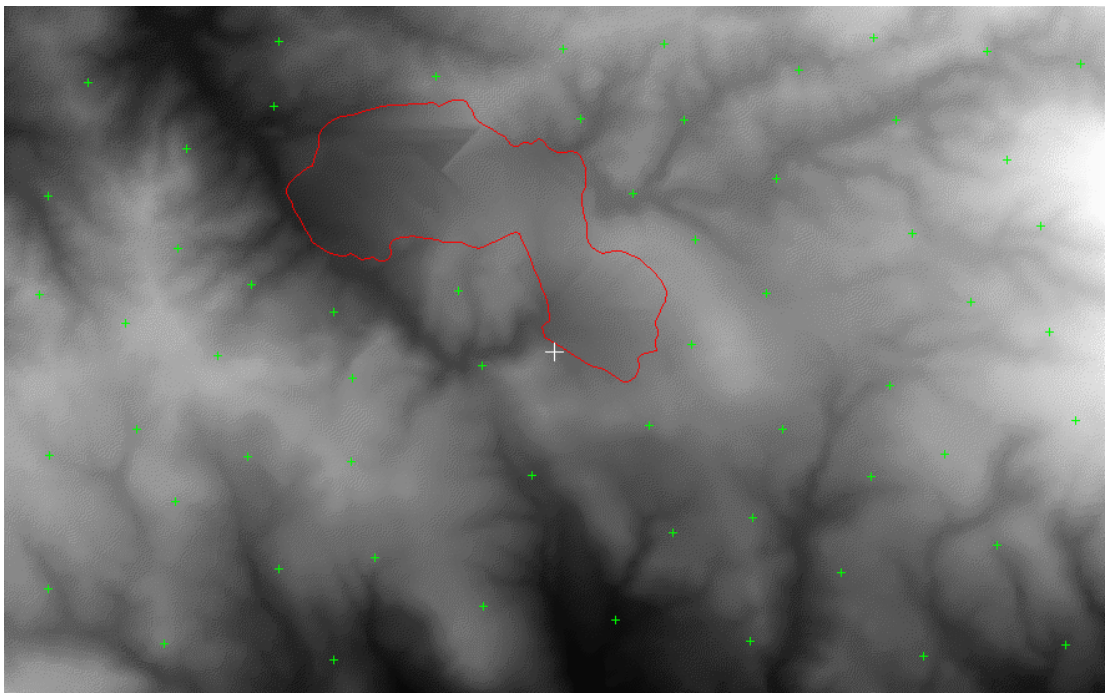

Figure 4. The locations of spot heights in the reference DEM used to calculate the RMS Error of elevations against the extracted SPOT DEM. Red line shows the extent of the Ferro-Nickel Mine in 1990 (see Figure 1). Notice the interpolation effects inside the mine area.

RESULTS

Accuracy Assessment of the SPOT PAN DEM

In the following table (Table IV) the vertical accuracy of the SPOT DEM is calculated using 60 check points randomly selected. The reference heights originated from the reference 10-m DEM of 1990. (see Figure 4). Both DEMs share the same cartographic projection (projection UTM, Zone 34, ellipsoid International 1909, datum European 1950), so the identification of the check points could be done with sub-pixel accuracy. The z-RMSe was 15.74 m (see Table IV) which is a figure comparable to the ones found in the bibliography for mountainous areas (e.g. Giles and Franklin, 1996; Devereux et al., 1997).

A more stringent, one-to-one pixel comparison (Figure 5) of the SPOT DEM with the 10 m, reference DEM yielded a mean error of -3.5 m and a standard deviation of 21.2 m (Figure 6). The difference image (Figure 5) shows only two areas of high intensities, a bright one towards the top and a dark one towards the bottom. The high error in the top is due to the lack of proper reference data (see artifacts inside the red polygon in Figure 4). The SPOT DEM has also overestimated heights in other areas (see bright patches), however, the majority of the differences is negative. Nevertheless, the lack of systematic trends or patterns in the error, the small mean error and standard deviation (given the large size of the sample; 491175 pixels, see statistics in Figure 6) indicates that the SPOT DEM may be used to produce orthoimagery.

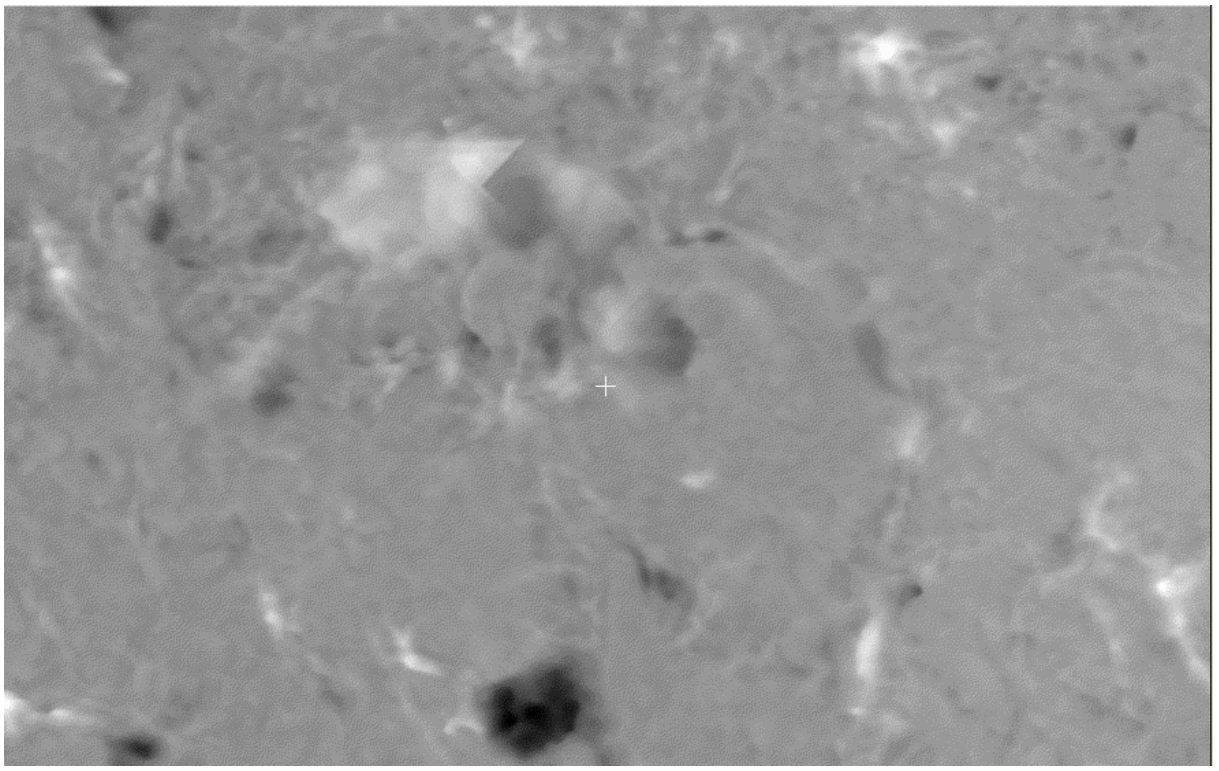

Figure 5. Intensity map of the difference image SPOT DEM (Figure 3) minus Reference DEM (Figure 4). Bright areas indicate positive differences, dark areas the opposite. Pixel size 10-m. The irregular texture in the upper-centre part of the image results from the lack of elevation data in the original map (Figure 1) that was used to produce the reference DEM.

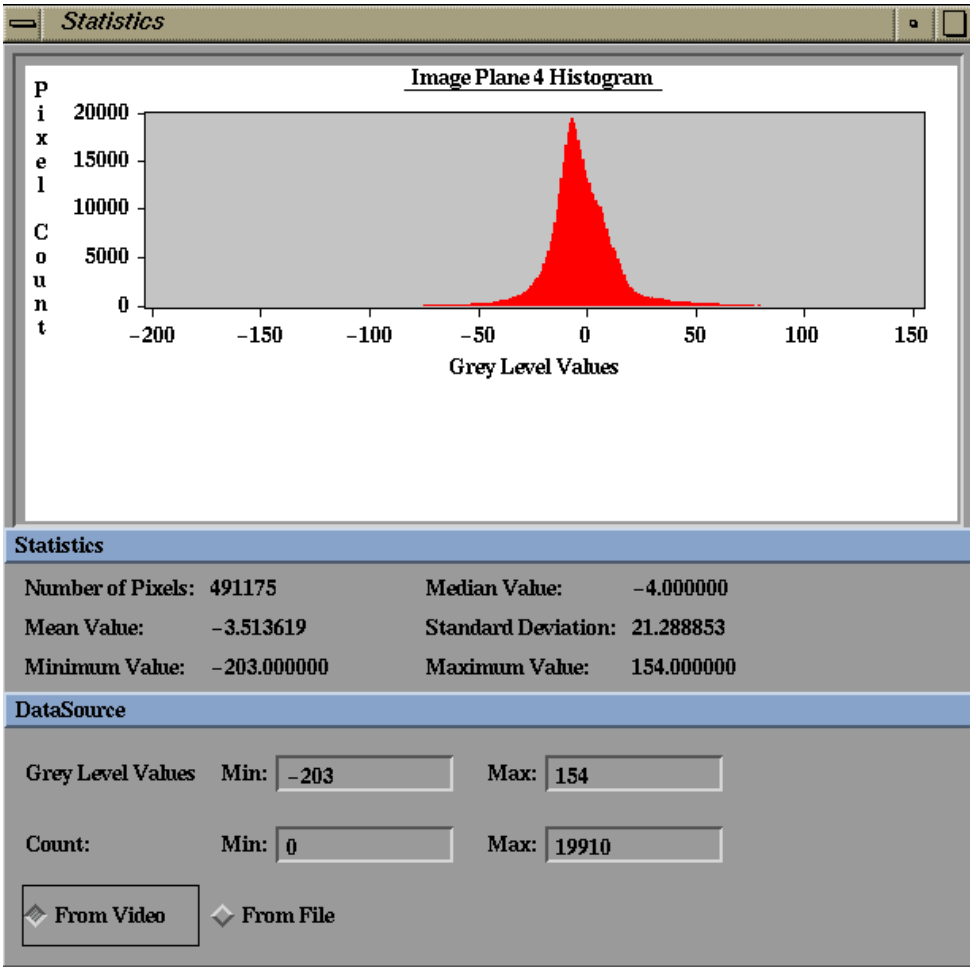

Figure 6. Descriptive statistics and the histogram of the difference image of the SPOT DEM minus the Reference DEM. Pixel size of all images 10-m. The difference image shows a negative mean error and a standard deviation of about 21 m.

Production of Orthoimagery

Two orthoimages for central Evia were produced using the reference DEM (procedure 1) and applying the EASI module SORTHO with Nearest Neighbour Resampling. The test window is shown in the shaded relief image of Figure 7 (red box) which demonstrates the rugged relief of that area (Figure 7 resulted from the Figure 4 dataset after applying an illumination source of a sun azimuth of 180 degrees and a sun elevation of 45 degrees). The right orthoimage (16 January 1993) is shown in Figure 8, while the left orthoimage (4 February 1993) is shown in Figure 9. A qualitative comparison of these two figures indicates that the orthorectification of the right image is better than that of the left one. The difference is due to the influence of GCP quality and distribution and secondly, the greater view angle of the HRV sensor in the left image (29 degrees off nadir). The comparison can be visually assessed by overlying a set of two vector layers originating from the map of Figure 1. These vectors are the main roads in this region (major roads are shown in red and minor roads are shown in green colour). For a large distance along the road (look inside the cyan circle on the Figures 8 and 9) the mean error of the right image is about 2 pixels (20 m) whereas the error of the left image averages about 3 pixels (30 m). Maximum errors in the same area are 5 pixels for the right image and 9 pixels for the left image. Note that the thickness of the road-vector line on the map (Figure 1) is about half a millimetre (1 mm equals 50 m) or 25 metres on the ground (roads in Evia are narrower that 25 m), but the digitising accuracy of an average operator is about 0.1 of a millimetre or 5 metres on the ground, bringing the maximum, cumulative digitisation error to 30 m (or 3 SPOT PAN pixels). This characteristic further reduces the positional error of the road on the right image with respect to the vector trajectory. Therefore, SPOT PAN orthoimages produced by use of the spaceborne DEM are expected to show spatial characteristics similar to those in Figures 8 and 9.

DISCUSSION

Our results indicate that the spaceborne DEM can be used in the orthorectification procedures of SPOT 1A imagery without significant compromises in the quality of the correction. For most geological applications the use of either dataset such as that of Figure 3 or Figure 4 would suffice to produce orthoimagery of acceptable quality to draw lithological boundaries for 1:50,000 scale mapping. Moreover, the SPOT dataset can be updated regularly (twice a year) at a reproduction rate that cannot be matched by the reference DEMs (usually reproduced every ten years). This repetitive advantage of the SPOT DEM is of critical importance for many geologic applications, which require up-to-date orthoimagery.

However, problems often encountered during the production of spaceborne DEMs are :

1) many times only low-sun angle (winter time) stereopairs are available for the time period of interest. Although these stereo-pairs yield good B/H ratios, the extensive shadows over the images cause the stereomatching algorithm to fail locally.
2) images with very-high off-nadir angles (> 25 degrees) do not help to locate many GCPs at the sub-pixel level because of excessive distortions
3) non-optimum distribution of GCPs across the images or the topographic map due to the lack of clearly identifiable man-made features in areas of moderate and high relief and
4) degraded accuracy of GCPs in some topographic maps due to inherent, bad map quality (where elevation errors of 10 m and planimetric errors of $\geq$ 15 m are often found).

In areas of moderate relief, the choice of the rectification method depends on the output scale of mapping and the available budget. Indeed, budget constraints may necessitate the use of the traditional (polynomial) method. Orthoimages are a time (i.e. money) consuming production activity when compared with non-parametric rectifications. Our experience indicates that for 2^{nd} order polynomial transformations for an area 50×50 kilometres (size of a TM miniscene; cost in Europe between 800 - 1400 Euros), the time required to achieve a XY RMSe ≤ 1 pixel (at the GCPs) is between 3-4 hours. This time can only be achieved using OrthoProcedures when a high-resolution geocoded DEM is available from external sources. Other geocoding work at IIS with Landsat 5 TM data for the same area (see Figure 10) confirmed what is already known from other studies (e.g. Cheng and Toutin, 1995), that the internal geometric characteristics of the TM orthoimages were much better than those on images rectified with polynomials. For example, coastlines, drainage and cultural features on the 1:50,000 topographic maps matched (on average) within 1-2 TM pixels their counterparts on the orthoimages, whereas the average matching for the polynomial image was around 3 TM pixels.

As new high resolution sensors are about to collect along-track stereo imagery (such as ASTER; Abrams and Hook, 1995) new emerging markets for Orthoimagery may be identified : a) the environmental geosciences field where accurate raster data are usually needed to identify suitable areas for industrial waste disposal (and many other applications) and b) the geoInformation - geography field where land-use and slope maps become parts of the user requirements for territorial risk assessments and telecommunication networks. Furthermore, the small mean error of the SPOT DEM with respect to the reference DEM (Figures 5 and 6) indicates that this method may be also applied towards extracting volumetric information in the geosciences.

Figure 7. Shaded Relief image of the central Evia (Greece) demonstrating the rugged relief of the area. Illumination is from the south (180) at 45 degrees elevation. Red box indicates the orthorectified window of the 1993 SPOT stereopair.

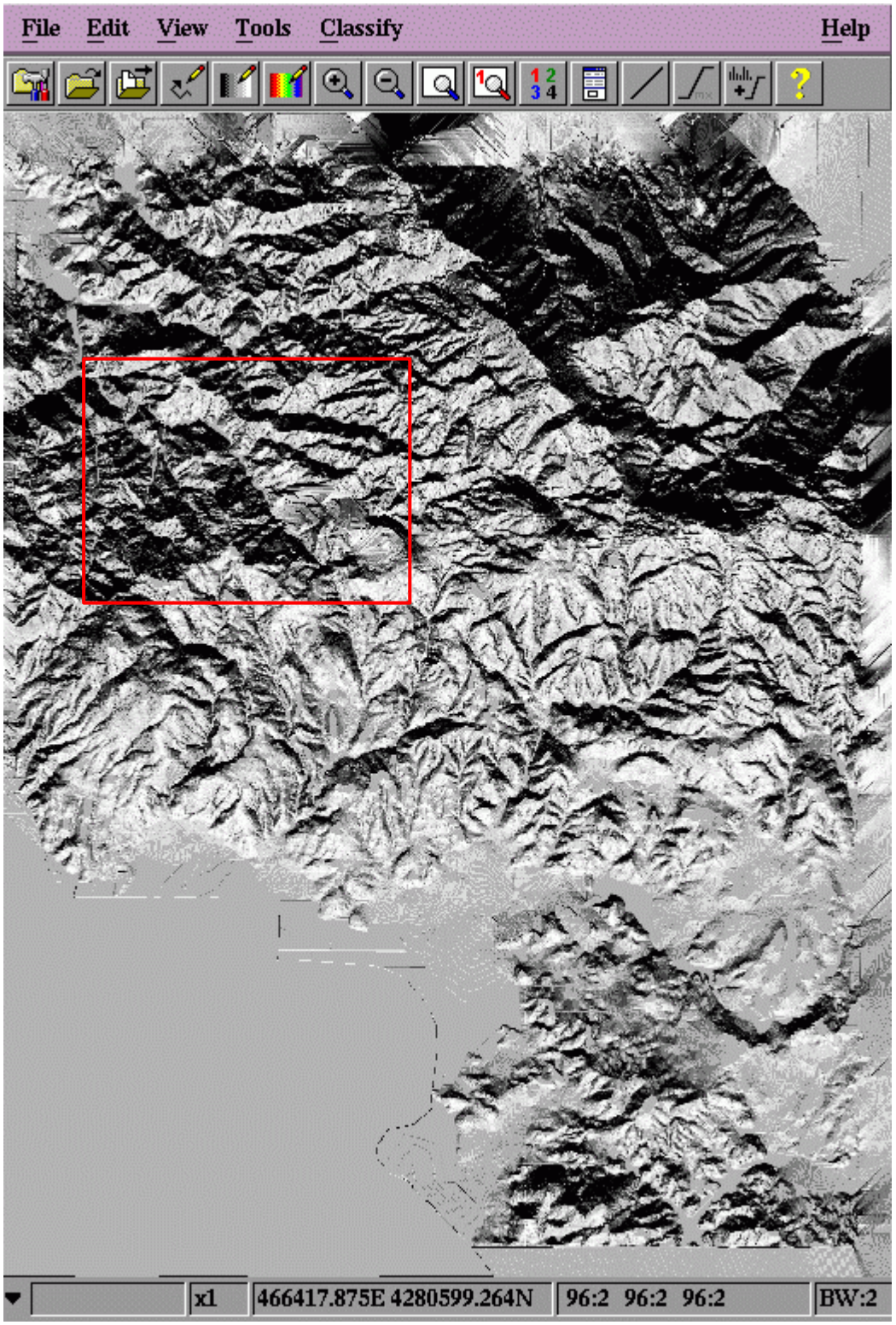

Figure 8. SPOT PAN orthoimage of the 16 January 1993 of central Evia, Greece (see image characteristics in Table I below). Red and green lines are digitised roads. Notice the good fit of the red line and the bright linear below it. Elevations range between 290 - 687 metres.

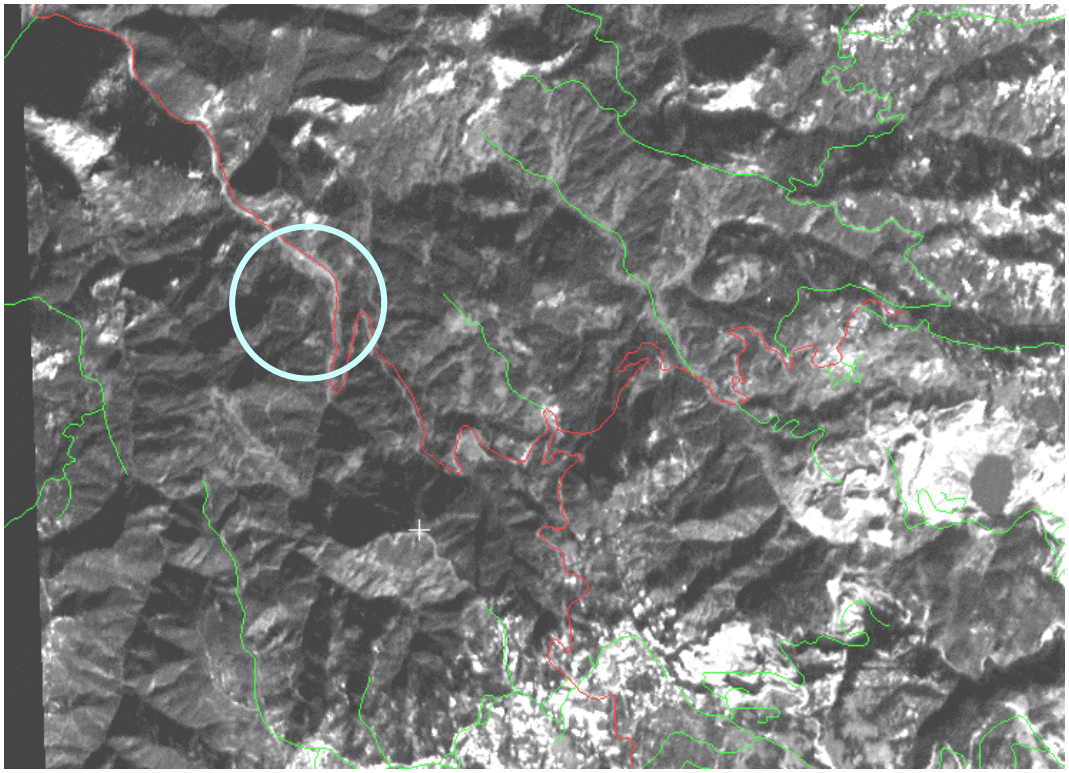

Figure 9. SPOT PAN orthoimage of the 4 February 1993 of central Evia, Greece (see image characteristics in Table I below). Red and green lines are digitised roads. Notice the systematic deviation to the right of the red line with respect to the bright linear below it. Elevations range between 290 - 687 metres.

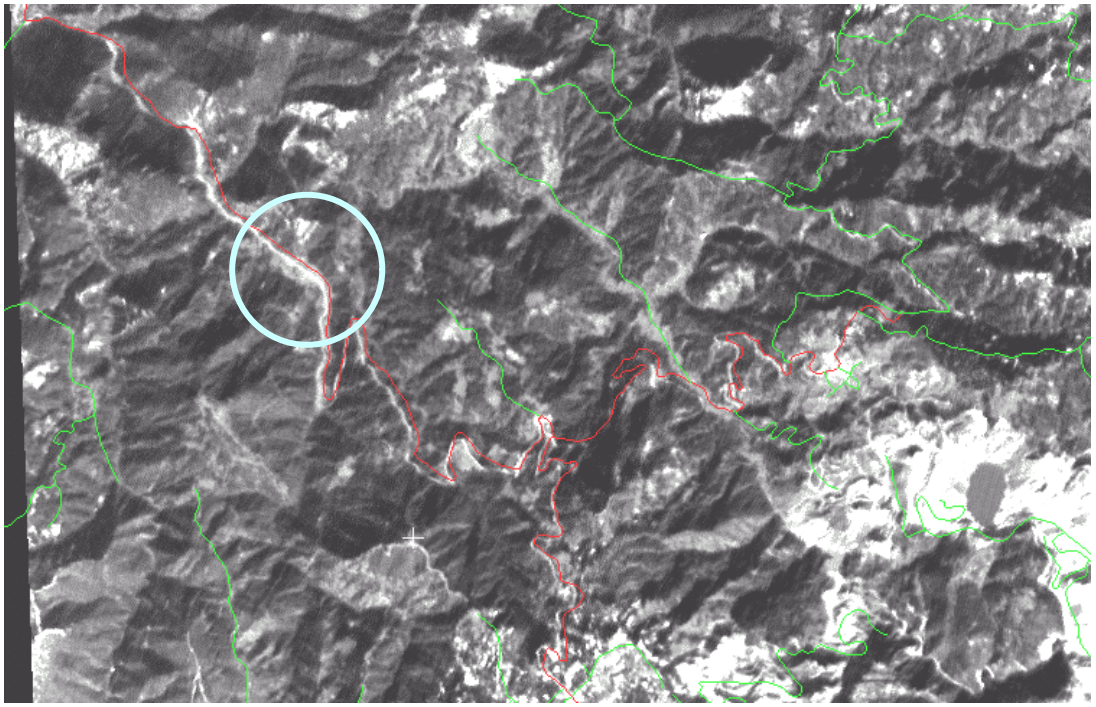

Figure 10. Image Map showing a geocoded Landsat 5 TM 321 image of Evia (central Greece - 18/4/97) by use of a 3rd -order polynomial (34 GCPs, RMSe x=1.13, y=0.69 pixels). The overlain vectors depict roads and drainage lines matching the corresponding image features on average about 3 TM pixels. Cyan box indicates the orthorectified SPOT window extent.

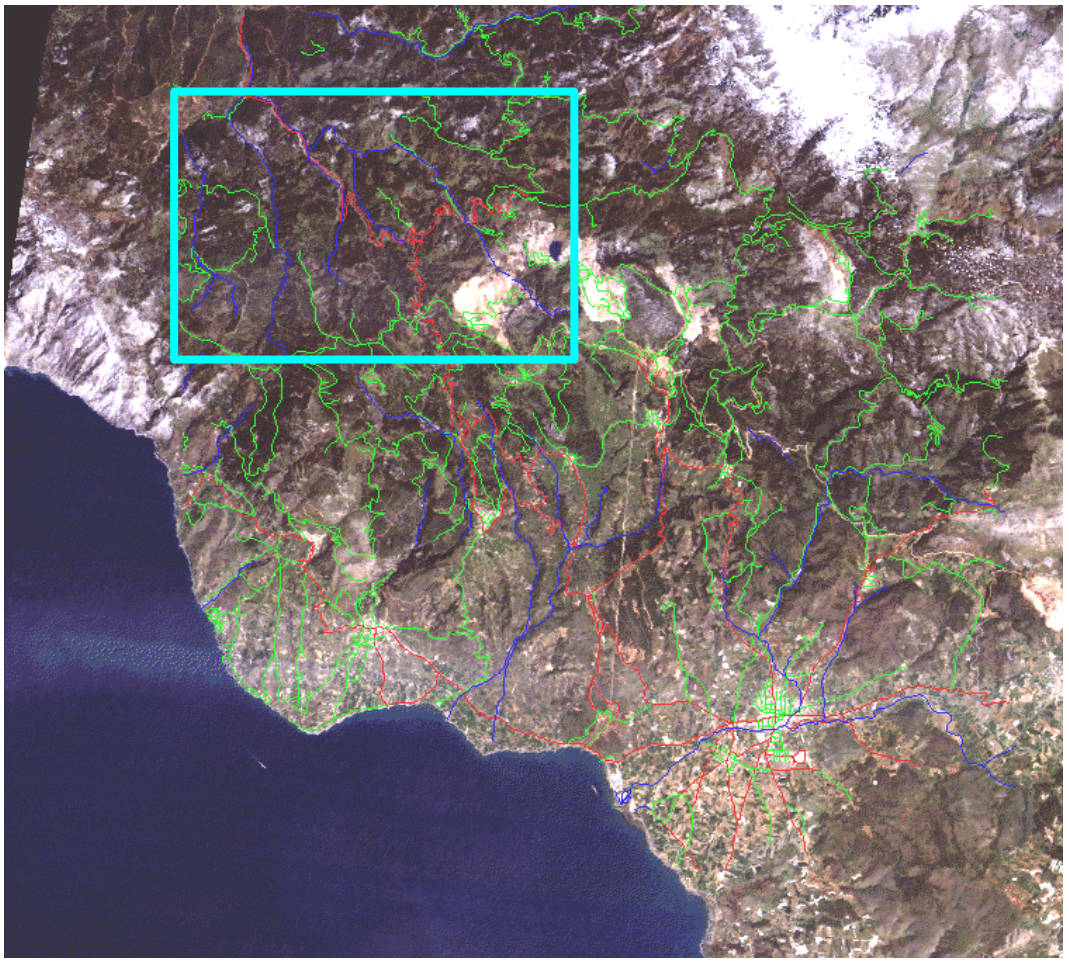

CONCLUSIONS

If the cost of extracting spaceborne DEMs for OrthoImagery can be sustained then it is recommended that this procedure be used instead of digit-DEMs or polynomials for all geological work at scales 1:50,000 (and smaller) in areas of moderate-high relief. The implementation of procedure 1 (high-resolution, reference DEM) is usually an order of magnitude more expensive than the spaceborne DEM. Our work demonstrated that SPOT1A-derived DEMs with a 56 degrees angular separation had a 3.5 m mean error when compared to 10-m reference (digit) DEMs. This figure may be also useful for attempting to extract volumetric information.

ACKNOWLEDGEMENTS.

We are thankful to Dr Cheng and Dr Toutin of PCI Geomatics for their useful comments and to Prof G. Petrie for provision of extensive bibliography. The Evia SPOT PAN 1A stereopair acquisition was funded by the EU/DGXII ENV4-CT96-0373 ASTERISMOS project (www.iis.gr/asterismos). An earlier version of this paper was presented by AG at GRSG 98 in Oxford, UK. We thank the IIS SA Managing Director Mr Yannis Cobopoulos for permission to publish this paper.

REFERENCES

Abrams, M., and Hook, S. J., 1995. Simulated ASTER data for Geologic Studies. IEEE Transactions on Geoscience and Remote Sensing, vol 33 (3), p. 692 - 699.

Al-Rousan, N., Cheng, P., Petrie, G., Toutin, Th., and Zoej, M. L. V., 1997. Automated DEM extraction and Orthoimage generation from SPOT Level 1B imagery. . Photogrammetric Engineering and Remote Sensing, vol 63, no 8, p. 965 - 974.

Al-Rousan, N., and Petrie, G., 1998. System Calibration, geometric accuracy testing and validation of DEM & Orthoimage data extracted from SPOT stereopairs using commercially available Image Processing Systems. IARPS, vol 32, Part 4 "GIS-Between Visions and Applications", Stuttgart, p. 8-15.

Carrara, A., 1988. Drainage and Divide Networks derived from high-fidelity Digital Terrain Models. In : C.F. Chung et al., (eds.), Quantitative Analysis of Mineral and Energy Resources, NATO ASI Series C Mathematical and Physical Sciences, vol 223, 581 -597.

Cheng, P., and Toutin, T., 1995. High Accuracy Data Fusion of Satellite and Airphoto Images. ACSM/ASPRS Annual Convention & Exposition technical papers, volume 2, 453 - 464.

Densmore, A. L., Ellis, M. A., and Anderson, R. S., 1998. Landsliding and the evolution of normal-fault-bounded mountains. Journal of Geophysical Research, vol. 103, no B7, p 15203 - 15219.

Devereux, B. J., Costa-Posada, C. R., and Amable, G. S., 1997. Land cover and hydrology of the Messara catchment, Crete. P 23rd Annual Conference and Exhibition of the Remote Sensing Society Proceedings, p. 243 - 248.

Dymond, J. R., DeRose, R. C., and Trotter, C. M., 1992. DTMs for Terrain Evaluation. Geocarto International, 2, 53 - 58.

Ganas, A., White, K., and Wadge, G., 1997. SPOT DEM Analysis for fault segment mapping in the Lokris region, central Greece. EARSeL Advances in Remote Sensing Yearbook, volume 5, p. 46-53.

Giles, P. T., and Franklin, S. E., 1996. Comparison of derivative topographic surfaces of a DEM generated from stereoscopic SPOT images with field measurements. Photogrammetric Engineering and Remote Sensing, vol 62, no 10, p. 1165 - 1171.

Gugan, D. J., and Dowman, I. J., 1988. Topographic mapping from SPOT imagery. Photogrammetric Engineering and Remote Sensing, vol 54, no 10, pp. 1409 - 1414.

HAGS (Hellenic Army Geographic Service), 1990. 1:50000 topographic map "Psachna Sheet".

Husak, G. J., Hadley, B. C., and McGwire, K. C., 1999. Landsat Thematic Mapper registration accuracy and its effects on the IGBP validation. Photogrammetric Engineering and Remote Sensing, vol 65, no 9., pp. 1033 - 1039.

Johnson, C. A., and Harrison, C. G. A., 1989. Tectonics and volcanism in central Mexico: A Landsat Thematic Mapper Perspective. Remote Sensing Environment, vol 28, p 273 - 286.

Massonnet, D., Rossi, M., Carmona, C., Adragna, F., Peltzer, G., Feigl, K., and Rabaute, T., 1993. The displacement field of the Landers earthquake mapped by radar interferometry. Nature, vol 364, p. 138-142.

Muller, J.-P., 1989. Real-Time stereomatching and its role in future mapping systems. Surveying and Mapping 89, University of Warwick, 17-21April 1989, p. 1-15.

Petrie, G., 1998. Space Imagery for Topographic Mapping. GeoInformatics (April/May 1998), p. 24 - 33.

Rao, T. Ch. M., Rao, . V., Kumar, A. R., Rao, D. P., and Deekshatula, B. L., 1996. Digital Terrain Model (DTM) from Indian Remote Sensing (IRS) Satellite Data from the overlap area of two adjacent paths using digital photogrammetric techniques. Photogrammetric Engineering and Remote Sensing, vol. 62, no 6, p. 727-731.

Tibaldi, A., and Ferrari, M., 1988. Potential of Landsat Thematic Mapper image for crystalline rock type discrimination : Gregory Rift, Kenya. Geocarto International, 1, p 3 - 12.

Toutin, T., 1998. SPOT and Landsat Stereo Fusion for data extraction over mountainous areas. Photogrammetric Engineering and Remote Sensing, vol 64, no 2, pp. 109-113.

Zoej, M. J. V., and Petrie, G., 1998. Mathematical Modelling and accuracy testing of SPOT Level 1B stereopairs. Photogrammetric Record, vol 16 (91), p. 67 - 82.

Table I – SPOT Data characteristics

	SPOT 1A 16/1/1993	SPOT 1A 4/2/1993
Scene Identification	S2H1930116090905	S2H2930204094347
Scene centre latitude (deg)	0.3881528D+02	0.3881528D+02
Scene centre longitude (deg)	0.2351472D+02	0.2383889D+02
Angle of Incidence (deg)	R26.9	L28.9
HRV mirror stepping no.	9	90
Sensor	HRV PAN mode	HRV PAN mode
Scene Size	60 x 60 km	60 x 60 km
Resolution (nadir)	10 m	10 m
Scene Orientation Angle (deg)	008.3	014.4
Sun Angle (Azimuth)	157.3	164.2
Sun Angle (Elevation – deg)	027.0	033.4
Date Time	16/01/1993 09h 09′ 05′′	04/02/1993 09h 43′ 46′′
H0 (Sensor Height)	0.8302972000000000D+06	0.8301308000000000D+06
Angular Separation R-L look	55.8	
Base/Height ratio	1.05936	

Table II - GCP report for the image file sp040293.pix

GCP Id	Uncorrected X	Uncorrected Y	Georef (EGSA) X	Georef (EGSA) Y	Elevation
12	2798.18750	5738.56250	475009.08983	4270452.75340	119.0
26	1693.18750	4930.43750	463749.09499	4281703.03730	427.46670
4	1740.531250	5461.406250	462781.76342	4276470.56990	316.79990
5	2301.31250	5850.68750	468601.71539	4270963.54950	39.155130
6	1898.406250	5657.343750	464218.39446	4274095.36800	133.95490
38	1149.12500	4479.12500	458657.03608	4287676.15910	107.95310
8	2012.093750	5867.968750	464971.82763	4271713.78120	136.94020
9	2025.93750	5972.31250	464844.12709	4270663.45680	80.00
10	2188.281250	5974.468750	466871.37311	4270114.35100	22.972210
11	2534.87500	5845.12500	471490.94004	4270254.81990	39.00
31	2277.62500	5837.87500	468349.50683	4271145.52060	47.00
24	2039.031250	5473.593750	466395.68861	4275410.66800	263.48490
2	2833.93750	5640.81250	475721.02032	4271295.56690	137.00
15	2829.56250	5754.43750	475363.45882	4270206.93280	119.00
33	2757.18750	5545.56250	475044.20748	4272448.05060	176.20220
29	2454.37500	5576.87500	471219.57640	4273089.73820	183.00
37	2916.37500	5463.87500	477215.11660	4272713.02610	238.63000
36	2889.12500	5440.62500	476946.94548	4273025.88870	261.26870
34	2985.62500	5551.62500	477847.23426	4271659.50920	139.82590

RMS Error (pixels) X: 0.78 Y: 0.79

Table III - GCP report for the image file sp160193.pix

GCP Id	Uncorrected X	Uncorrected Y	Georef (EGSA) X	Georef (EGSA) Y	Elevation
1	4027.43750	5415.56250	464847.31960	4270663.45680	80.00
2	4016.43750	5308.43750	464975.02014	4271713.78120	136.76050
25	4493.656250	4858.968750	471640.98817	4275251.04420	221.92600
4	4959.12500	5380.62500	476059.42674	4269316.23210	119.00
34	3242.2500	3815.2500	458666.61362	4287672.96670	108.38070
37	3579.87500	4574.37500	461415.36768	4279653.46800	515.23510
28	4174.12500	4898.87500	467784.43195	4275417.05290	319.88350
27	4469.37500	5173.62500	470651.30901	4272211.80740	123.19770
24	3839.37500	5393.37500	462634.90780	4271218.94750	36.00
29	3782.37500	4921.37500	463021.20193	4275918.27160	292.84420
11	4337.62500	5485.62500	468387.81699	4269412.0640	20.762460
22	3990.406250	5240.906250	464809.09440	4272416.12590	158.60500
32	3467.2500	4845.2500	459586.05749	4277204.83920	721.88370
14	4327.12500	5329.62500	468598.52288	4270966.74200	39.522910
35	3737.468750	4333.156250	463749.09499	4281703.03730	427.46670
23	3903.37500	5111.12500	464017.26612	4273846.35490	152.6010
17	4895.62500	5380.87500	475299.60855	4269431.16120	106.46580
20	5047.406250	5115.468750	477693.99362	4271752.09100	173.84330
33	3453.12500	4443.12500	46045.779420	4281173.08640	287.29520

RMS Error (pixels) X: 0.70 Y: 0.78

Table IV – Accuracy assessment of the SPOT derived DEM

Id	UTM X	UTM Y	Ref DEM m	SPOT DEM m	Ref - SPOT DEM m	(Ref DEM – SPOT DEM)^2
1	722526.9	4284299.7	412	396	16	256
2	723315.5	4283769.7	438	416	22	484
3	722205.3	4283395.5	435	417	18	324
4	723242.8	4282969.4	548	519	29	841
5	722132.7	4282605.6	598	563	35	1225
6	722817.5	4282377.0	633	624	9	81
7	723834.2	4282678.4	469	446	23	529
8	724487.8	4282460.1	430	410	20	400
9	723564.5	4282117.2	610	614	-4	16
10	722910.8	4281524.7	563	561	2	4
11	722215.7	4281316.9	595	585	10	100
12	723222.1	4280942.7	573	558	15	225
13	722205.3	4280246.4	506	489	17	289
14	723128.7	4279799.5	506	479	27	729
15	724052.1	4280402.3	426	426	0	0
16	723803.1	4281306.5	517	510	7	49
17	724643.5	4281930.1	560	551	9	81
18	725494.2	4282636.8	499	484	15	225
19	725681.0	4282034.0	437	438	-1	1
20	724633.1	4281264.9	582	570	12	144
21	724819.9	4280495.8	466	456	10	100
22	724487.8	4279674.7	317	309	8	64
23	726085.6	4281150.6	370	364	6	36
24	726749.6	4279996.9	239	226	13	169
25	725691.4	4280100.9	454	434	20	400
26	727019.4	4281555.9	494	501	-7	49
27	727216.5	4280693.3	411	408	3	9
28	727828.6	4279820.2	373	366	7	49
29	727849.4	4280818.0	452	452	0	0
30	728088.0	4281524.7	494	492	2	4
31	727361.8	4282200.3	571	569	2	4
32	728803.9	4281140.2	481	483	-2	4
33	728565.3	4280371.1	427	433	-6	36
34	729218.9	4279705.9	400	396	4	16
35	730360.2	4279789.1	349	362	-13	169
36	729810.3	4280589.3	491	520	-29	841
37	729395.3	4281327.3	615	621	-6	36
38	730443.2	4281597.5	739	750	-11	121
39	728949.2	4281878.1	539	563	-24	576
40	730235.7	4282304.2	724	735	-11	121
41	729602.8	4282543.3	640	649	-9	81
42	727392.9	4283042.2	558	548	10	100
43	727963.5	4282616.0	539	541	-2	4
44	728046.5	4283530.6	507	507	0	0
45	726894.9	4283416.3	498	486	12	144
46	727299.5	4283998.3	495	486	9	81
47	726469.5	4284008.7	499	480	19	361

48	726334.6	4284570.0	593	606	-13	169
49	725307.5	4284351.7	520	507	13	169
50	724052.1	4284632.3	376	373	3	9
51	724010.6	4284112.7	315	300	15	225
52	728222.9	4284403.7	562	624	-62	3844
53	729001.0	4283998.3	567	572	-5	25
54	729135.9	4283094.1	626	631	-5	25
55	730163.1	4283156.5	712	714	-2	4
56	729893.3	4283686.5	732	738	-6	36
57	730484.7	4284455.6	637	642	-5	25
58	729727.3	4284549.2	638	617	21	441
59	728824.7	4284663.5	669	670	-1	1
60	727143.9	4284611.5	597	615	-18	324

RMS Error (SQRT [Σ (ref-SPOT DEM)^2/n]): 15.74 m